# Accepted Manuscript


3D-structured multi-walled carbon nanotubes/copper nanowires composite as a porous current collector for the enhanced silicon-based anode

Yinchao Zhao, Chenguang Liu, Yi Sun, Ruowei Yi, Yutao Cai, Yinqing Li, Ivona Mitrovic, Stephen Taylor, Paul Chalker, Li Yang, Cezhou Zhao

PII: S0925-8388(19)32393-X

DOI: https://doi.org/10.1016/j.jallcom.2019.06.302

Reference: JALCOM 51201

To appear in: *Journal of Alloys and Compounds*

Received Date: 17 January 2019

Revised Date: 10 May 2019

Accepted Date: 24 June 2019

Please cite this article as: Y. Zhao, C. Liu, Y. Sun, R. Yi, Y. Cai, Y. Li, I. Mitrovic, S. Taylor, P. Chalker, L. Yang, C. Zhao, 3D-structured multi-walled carbon nanotubes/copper nanowires composite as a porous current collector for the enhanced silicon-based anode, *Journal of Alloys and Compounds* (2019), doi: https://doi.org/10.1016/j.jallcom.2019.06.302.

# 3D-structured Multi-walled Carbon Nanotubes/Copper Nanowires Composite as a Porous Current Collector for the Enhanced Silicon-Based Anode

Yinchao Zhao[ab], Chenguang Liu[ab], Yi Sun[ab], Ruowei Yi[cd], Yutao Cai[ab], Yinqing Li[e], Ivona Mitrovic[a], Stephen Taylor[a], Paul Chalker[f], Li Yang [d*], Cezhou Zhao[b*]

[a] *Department of Electrical Engineering and Electronics, University of Liverpool, Liverpool L69 3GJ, United Kingdom*

[b] *Department of Electrical and Electronic Engineering, Xi'an Jiaotong-Liverpool University, Suzhou 215123, China*

[c] *Stephenson Institute for Renewable Energy, Department of Chemistry, University of Liverpool, Liverpool L69 7ZD, United Kingdom*

[d] *Department of Chemistry, Xi'an Jiaotong-Liverpool University, Suzhou, Jiangsu 215123, China*

[e] *Dongguan Hongde Battery Ltd.Co., Dongguan 523649, China*

[f] *Centre for Advanced Materials, University of Liverpool, L69 3GH, United Kingdom*

[*]Corresponding authors.

E-mail addresses:
li.yang@xjtlu.edu.cn (L. Yang); cezhou.zhao@xjtlu.edu.cn (C. Zhao).

## Abstract

In this study, multi-walled carbon nanotubes/Cu nanowires-coated on the copper foil used as a three-dimensional porous current collector for Si electrode has been developed to tackle the problems of silicon-based lithium-ion batteries. The highly conductive Cu nanowires cooperated with robust multi-walled carbon nanotubes not only improve the inferior electric conductivity of the Si anode but also strengthen the total frame stability. Furthermore, the three-dimensional structure creates numerous voids on the surface of Cu foils. Such porous structure of the modified current collector offers the flexible volume expansion during lithiation/delithiation process. Meanwhile, the core-shell structure of multi-walled carbon nanotubes/Si and Cu nanowires/Si minimizes the deformation strain and greatly improves the long-term cycling performance in a real battery. As a result, a high specific capacity of 1845 mAh $g^{-1}$ in a half cell at a current density of 3.5 A $g^{-1}$ after 180 cycles with a capacity retention of 85.1 % has been achieved without any conductive additives or binder. The demonstrated three-dimensional current collector coupled with Si anode might inspire new material development on high-performance of lithium-ion batteries.


**Key words:** Si-based lithium-ion batteries; copper nanowires; multi-walled carbon nanotubes

# 1. Introduction

With the increased demand to widely substitute the renewable and reliable energy for the conventional fossil fuels, lithium-ion batteries (LIBs) have been considered as the most promising candidate due to its high energy density, excellent cyclic performance, and environmental benignity. Indeed, extensive applications of LIBs are witnessed in the market, for example in hybrid electric vehicles, portable electronic equipment, and other energy storage fields. However, the low theoretical capacity of commercialized graphite anodes (372 mAh $g^{-1}$) for LIBs are far from meeting the tremendous demands created by the fast-growing market [1]. Therefore, enormous efforts have been focused on investigating the desirable electrode materials with better recyclability and advanced capacity for next-generation LIBs.

Among a wide variety of emerging electrode materials, silicon (Si) is regarded as an outstanding and appealing anode material for LIBs. It complies with the alloying/de-alloying mechanism in which 15 Li atoms occupy, on average, 4 Si atoms to form the lithium-Si alloy ($Li_{15}Si_4$) [2]. Moreover, Si has an advantage in its substantial reserves in the world as well as being environmentally friendly element. Consequently, Si anodes are well known for its extremely high theoretical gravimetric capacity (3579 mAh $g^{-1}$) and volumetric capacity (9786 mAh $cm^{-3}$) at room temperature, respectively, both of which exceed that of any other anode materials [3]. Despite all these advantages, challenges still remain to facilitate the practical applications or mature commercialization of Si-based LIBs. The great volume expansion (about 300 %) of Si during the lithium ions insertion/extraction cycling produces a huge internal stress [4]. Subsequently, dramatic pulverization and cracking will occur, followed by a weak electrical contact between active materials and current collectors [1]. Furthermore, the solid-electrolyte interphase (SEI) covering the surface of the electrode is fragmented with Si shrinking and regenerated when the fresh surface approaches the electrolyte again [4]. As a result, the repetitive fragmentation and regeneration process produce a thick and unstable SEI layer, leading to a low transport efficiency of Li ions [5]. Another critical challenge is the poor conductivity of Si, which is a constrain for the electrochemical reaction kinetics and rate capability performance. All of these problems cause a fast and continuous capacity decline of the silicon-based electrode during a long-term cycling [6].

To address these issues, one popular approach is to contrive the nanostructured Si materials to accommodate the huge volume change, such as Si nanoparticles (NPs) [7], Si nanowires (NWs) [8], and Si nanotubes (NTs) [5, 9]. However, these strategies could merely relieve the strain for a short term without preventing the final pulverization of Si. Hence, encapsulating nanostructured Si with carbon or metal oxides materials has gained great attention for its highly improved electrochemical performance [10]. For instance, Wu *et al*. introduced Si NPs@CNTs with adequate interparticle space, exhibiting a high capacity around 1000 mAh $g^{-1}$ at 1 A $g^{-1}$ after 200 cycles [11]. In addition, the graphene film and $TiO_2$ were also explored to cover Si nanoparticles or microparticles so as to improve the uniform arrangement of active materials [7, 12]. These flexible shells could restrict the huge volume expansion of Si during cycling. Thus, the majority employed encapsulation layers are able to enhance the cycling lifespan of batteries. However, the above enhancements are commonly achieved at the expense of specific capacity because of small weight proportion of active materials, low Li storage in the outer layers, and the unsatisfactory conductivity. In terms of the overall electrode, the inactive materials including the current collector, conductive additives, binders, and other materials account for a large proportion of the mass and volume in the whole electrode, which considerably decreases the energy density of batteries [13]. Particularly, the polymer binders have a negative effect on the electronic conductivity of the overall electrode [14]. The recent strategy to tackle this challenge is to prepare active materials directly on the three-dimensional (3D)-structured conductive substrates such as copper foam [15, 16], nickel foam [17], carbon cloth [18, 19], and so on. The 3D binder-free anodes have been engineered to improve the electrochemical performance of the battery by removing the binders. On the other hand, the substrate, a 3D conductive network, not only improves the electrode conductivity by providing the fast transport paths for electron and ions but also provides excellent cycling life span by accommodating the volume expansion of active materials and anchoring them from failing off the substrate [20]. Hongxiang Wang and co-workers combined the Cu/amorphous Si (a-Si) core-shell nanowires with the flexible copper foam as a binder-free anode used in LIBs. The anode showed an excellent stable performance with only 0.03 % average capacity loss per cycle at 1 A $g^{-1}$ after 1000 cycles [21]. It is noted that the core-shell nanowires structure has been increasingly developed to further ameliorate the electrochemical performance of Si-based LIBs, such as Cu-Si [16, 22, 23] and Sn-Si [24] featuring conductive metal

as the core part. Zhang's group directly deposited Si film on Cu NWs anchored on a porous nickel foam and subsequently coated the Cu/Si core-shell nanowires with Ge films [25]. After 3000 cycles, Cu/Si/Ge composite retained a high specific capacity of 1523 mAh $g^{-1}$ at a specific current density of 1 A $g^{-1}$. These previous studies indicate that the electrochemical performance of Si-based anodes could be improved by constructing the metal/Si core-shell structure on a porous and flexible substrate.

In this work, the multi-walled carbon nanotubes (MWCNTs)/Cu nanowires (Cu NWs)/Si composite have been developed by depositing amorphous Si layer on the prepared porous current collector directly through a plasma-enhanced chemical vapor deposition (PECVD). The 3D porous MWCNTs/Cu NWs-coated Cu foil functions as a template for the subsequent deposition of Si layer. Interestingly, the composite exists in the form of Cu/Si and MWCNTs/Si core-shell structure simultaneously. By adjusting the number of spin-coating, different layers of MWCNTs/Cu NWs were achieved, which has significant impact on the cycling performance of electrodes. In addition, the weight ratio of MWCNTs and Cu NWs has been proved as an important factor affecting the cycling lifespan of electrodes. After 180 cycles, the MWCNTs/Cu NWs/Si composite shows a high specific capacity of 1842 mAh $g^{-1}$ at a current density of 1 A $g^{-1}$ and 1845 mAh $g^{-1}$ at 3.5 A $g^{-1}$, respectively. The corresponding capacity retentions are 93.4 % and 85.1 % after 180 cycles. The excellent performance demonstrates that MWCNTs/Cu NWs/Si composite can be used as a promising anode material for LIBs.

# 2. Experimental section

## 2.1 Synthesis of Cu NWs

The fabrication process of MWCNTs/Cu NWs/Si composite anode is depicted in Fig. 1. Initially, Cu NWs were synthesized according to the method reported by Chang's group [26]. Briefly, an aqueous solution of NaOH (322 mL, 15 M) was prepared in a beaker by magnetic stirring. When the reaction solution was cooled down to the ambient temperature, $CuSO_4 \cdot 5H_2O$ (28 mL, 0.1 M) and ethylenediamine (EDA) (2.6 mL, 99 wt. %) were added with constant stirring for 10 min. After that, 469 μL of hydrazine (35 wt. %) was added and stirred vigorously for further 10 min. The beaker was sealed and heated in an oil bath at 65 °C for 4 hours. Finally, the

Cu NWs were collected by centrifugation (8500 rpm for 10 min) and rinsed four times with deionized (DI) water and ethanol.

### 2.2 Preparation of Cu NWs and MWCNTs solution

The solution of Cu NWs dispersed in isopropyl alcohol (IPA) with the concentration of 25 mg/mL was prepared by ultrasonication for 1 hour. Concurrently, MWCNTs were dispersed in IPA (1 mg/mL) with an ultrasonic treatment for 3 hours. Subsequently, the above MWCNTs and Cu NWs solution were mixed by different weight ratios of MWCNTs and Cu NWs (MWCNTs: Cu NWs = 1:0, 1:1, 1:5, 1:10, 1:15, 1:50, and 0:1, w/w) with continuous stirring to achieve a homogenous solution.

### 2.3 Fabrication of porous current collector

For the porous MWCNTs/Cu NWs-coated current collector, the as-prepared mixture was spin-coated onto the Cu foils (2 cm × 2 cm) which had been pre-sonicated in acetone and ethanol to remove impurities on the surface. The parameters for spin-coating were set around 3000 rpm for 20 s. The desired layers of MWCNTs/Cu NWs on Cu foils were obtained by repeating spin-coating with different cycles. Between each spin-coating cycle, the substrates were dried in a vacuum oven at 80 °C for 10 min. In addition, pure Cu NWs and pure MWCNTs dispersed in IPA were respectively spin-coated on the Cu foils as the control groups following the same procedure.

### 2.4 Deposition of Si layer on MWCNTs/Cu NWs-coated Cu foils

The amorphous Si layer was deposited on the porous MWCNTs/Cu NWs-coated Cu foil by PECVD. During the deposition, the temperature was kept at 100 °C for 90 min under a flow of 35.5 sccm $SiH_4$ with the chamber pressure of 188 mTorr and RF power of 11 W. The mass loading of Si weighted between 0.12 and 0.18 mg $cm^{-2}$. Eventually, the as-prepared electrodes were annealed at 450 °C under 46 sccm $H_2$ flow (1.4 Torr) for 4 hours in low-pressure chemical vapor deposition (LPCVD), in order to reduce the copper oxide (produced during the preparation process) to copper.

According to different pre-coating materials, the samples were labeled with different abbreviations. PCS and PMS represent pure Cu NWs/Si (MWCNTs: Cu NWs = 0:1)

and pure MWCNTs/Si (MWCNTs: Cu NWs = 1:0) anodes. MCS1, MCS5, and MCS10 stand for the MWCNTs/Cu NWs/Si composites with 1:1, 1:5, 1:10, 1:15, and 1:50 different weight ratios of MWCNTs and Cu NWs, respectively.

### 2.5 Materials characterizations

The structure and morphology of the PCS, PMS and MCS composite electrodes were characterized using a scanning electron microscope (SEM, JEOL JSM-6510) with energy dispersive X-ray spectrometry (EDS) and transmission electron microscopy (TEM, Tecnai G2 F20S). The phase structure analysis was investigated by an X-ray diffraction system (XRD, D8 Advance, Bruker) with a Cu Kα radiation source (40 kV and 40 mA).

### 2.6 Electrochemical measurements

The composite electrodes were assembled into 2032-type coin cell in an argon-filled glove box (Vigor Sci-Lab) with lithium metal foil as the counter electrode and the polypropylene–polyethylene–polypropylene trilayer membranes (Celgard 2325) as the separator. The electrolyte of 1 M $LiPF_6$ dissolved in a mixture of dimethyl carbonate (DMC) and ethylene carbonate (EC) (1:1 by volume) was used. A galvanostatic charge/discharge cycling test was performed on a battery testing system (Neware CT-4008) in the voltage range of 0.01-2.0 V versus $Li^+/Li$ at different current densities. Cyclic voltammetry (CV) test was conducted at a rate of 0.1 mV $s^{-1}$ in the same potential range (0.01-2.0 V) on an Autolab electrochemical workstation (PGSTAT302N).

## 3. Results and discussion

To assess the optimal layer of Cu NWs coated on Cu foil, SEM images of Cu NWs with different layers by spin-coating are shown in Fig. 2a-d, respectively. For the fewer layers, Cu NWs look like a nest in the insert image of Fig. 2a and would be connected together with increasing cycles of spin-coating. It is found that the abundant Cu NWs intertwine together creating considerable internal void space for subsequently Si deposition. In Fig. 2a-b, the Cu NWs nests have dispersed over the surface of Cu foil with some exposed area. By contrast, 8 and 12 layers of Cu NWs

nearly cover the whole surface of Cu foils with more agglomerations, making the surface more uneven, as illustrated in Fig. 2c-d.

The electrochemical performance of the PCS electrodes with different spin-coated layers was examined, as shown in Fig. 3. It shows the first four CV curves at a scan rate of 0.1 $mV^{-1}$ with a potential window of 0.01-2.0 V. There is a broad peak around 0.63 V during the first cathodic scan, which corresponds to the generation of SEI layers. The reaction is irreversible because this peak disappears in the following cycles, indicating that the initial formation of SEI layers might prevent the contact between the active materials and electrolyte and restrain the further decomposition of electrolyte [27, 28]. Two intensive reductive current peaks at 0.19 V and 0.03 V are attributed to the insertion of Li ions into a-Si-matrix which causes the formation of amorphous $Li_xSi$ alloy and crystalline $Li_{15}Si_4$ alloy. During the anodic scanning, two oxidation current peaks around 0.44 V and 0.52 V are consistent with the two-step dealloying process ($Li_{15}Si_4 \rightarrow Li_xSi \rightarrow Li$). Little variation is observed in the sequent scanning cycles, which indicates a quite reversible and stable redox reaction of the electrode [21]. Particularly, the charge-discharge voltage profiles are exhibited in Fig. 3b. The first three cycles at 0.42 A $g^{-1}$ demonstrate the characteristic alloying/dealloying plateaus of the PCS anode. The discharge and charge capacities of the PCS electrode are 3173 and 2099 mAh $g^{-1}$ with an initial Columbic efficiency approaching 66.2 %. The large initial capacity loss is probably due to irreversible formation of the SEI layer [29].

In Fig. 3c, PCS electrodes with various layers of Cu NWs exhibit high cycling performance, which is superior to the electrode prepared by directly depositing Si film on the bare Cu foil (blue line). The planar Si/Cu foil electrode possesses the large initial capacity around 2456 mAh $g^{-1}$, but plummets to 500 mAh $g^{-1}$ after only 70 cycles with a retention of 20 %. By contrast, the porous pure Cu NWs-coated current collector provides tremendous space to accommodate the huge volume expansion of Si during cycling. The staggered network structure is beneficial to the fast transmission of Li ions. Hence, in comparison, the PCS composite could effectively mitigate the degradation of the Si-based lithium-ion batteries. It is also noted that the PCS electrode with 5 spin-coated layers of Cu NWs has the best cycling performance among the electrodes. Interestingly, the PCS electrodes with 8 and 12 coating layers (not shown in the figure) have more compact surface, but the resulting cycling

performance is unsatisfactory. The poor electrochemical performance of PCS electrodes with 8 and 12 coating layers may be attributed to the nonuniform deposition of Si by PECVD. When the thickness of Cu NWs increases with increasing the spin-coated layers, the Si tends to be deposited on the upper layers of Cu NWs, which leads to the uneven distribution of active materials. Besides, the thick Si on the upper layers would decrease the conductivity of the overall electrodes. These are probably the main reasons causing the low efficiency of electron transmission. Fig. 3d exhibits the rate capability of the PCS composite with 5 coating layers. The LIBs were tested at the current densities from 1 to 8 A $g^{-1}$ during the initial 120 cycles, with reversible discharge capacities of 1993, 1521, 1123, and 526 mAh $g^{-1}$. When the current density returns to 1 A $g^{-1}$, the electrode remains a capability of 1427 mAh $g^{-1}$ with a retention of 72 %. However, the electrochemical performance of PCS composite is unsatisfied since the capacity seriously declines after 60 cycles. One possible reason is that the Cu NWs with very fine diameter might be broken by the large strain during repeated cycling, which could be confirmed in SEM image of PCS electrode after 100 cycles (Fig. 8a) [30]. To enhance the mechanical stability, the robust MWCNTs were applied and cooperated with Cu NWs to form a stable and solid current collector.

The mixed solution of MWCNTs and Cu NWs with different weight ratios was spin-coated on the Cu foil to form the MWCNTs/Cu NWs-coated Cu foil which serves as a 3D porous current collector. The corresponding SEM images of MWCNTs/Cu NWs-coated Cu foils (MWCNTs: Cu NWs=1:10 and 1:1) with different spin-coated layers were compared in Fig. S1 and Fig. S2 respectively. For MWCNTs: Cu NWs=1:10, as shown in Fig. S1, it is clear that at low magnification the SEM images of MWCNTs/Cu NWs-coated Cu foils are similar to that of pure Cu NWs-coated Cu foils (Fig. 2). However, in Fig. S2e-f for MWCNTs: Cu NWs=1:1, there is still some exposed Cu foil surface in the SEM images of MWCNTs/Cu NWs-coated Cu foils with 8 coating layers, which we attribute to the large portion of MWCNTs in the mixture aggregating together, ultimately resulting in nonuniform distribution on the Cu foil. It is indicated that the MWCNTs/Cu NWs-coated Cu foils (MWCNTs: Cu NWs=1:10) show the uniform spin-coating surface owing to the appropriate weight ratio of MWCNTs and Cu NWs. Fig. 4a shows the SEM image of MCS1 electrode with 5 layers of MWCNTs/Cu NWs

(MWCNTs: Cu NWs = 1:1). Compared with the rigid Cu NWs, the MWCNTs with more flexible feature tend to enwind around the Cu NWs. The straight Cu NWs interlinked with the tortuous MWCNTs are beneficial to enhance the connection between the Cu NWs, which creates a 3D conductive framework as a good current collector. However, it is also observed that MWCNTs agglomerate together (marked as circle in Fig. 4a) to form large clusters, losing the porosity of the electrode. Thus, it is significant to balance the weight ratio of MWCNTs and Cu NWs on current collector. A single selected Cu/Si core-shell nanowire before annealing is shown in Fig. 4b, where the black core is encapsulated by grey shell. It could be estimated that the diameter of the original Cu NW is around 130 nm and the average thickness of Si shell is in the range of 10-50 nm according to Fig. 4b-c. After annealing in $H_2$ atmosphere, the Cu/Si core-shell structure involves empty space inside as illustrated in Fig. 4c. The hollow structure could be ascribed to reduction from CuO to Cu accompanied with the diffusion of Cu into the Si shell that is demonstrated in Fig. 4d [31], which is a capture of the boundary of the core-shell structure. The lattice spacing of 0.21 nm at the black part corresponds to the (111) plane of Cu [21, 25], and grey layer without lattice fringes represents the amorphous Si film, which are consistent with XRD results.

To qualitatively characterize the phase composites of the prepared electrodes, XRD was conducted. The XRD patterns of a Cu foil (black), Cu foil coated with MWCNTs/Cu NWs (red), and MCS1 before (blue) and after (brown) annealing are shown in Fig. 5. The patterns of all samples exhibit sharp and strong diffractions peaks emerging at 43.30°, 50.43°, and 74.13°, which are in good agreement to the face-centered cubic (fcc) Cu crystals (PDF#04-0836). For Cu foil coated with MWCNTs/Cu NWs and MCS1 before annealing, some minor peaks located at 35.54° and 38.71°are identified as CuO crystals (PDF#48-1548) and the peaks emerging at 36.42° and 42.30° are $Cu_2O$ crystals (PDF#05-0667), respectively. The diffraction peaks of CuO and $Cu_2O$ indicate that Cu NWs were partially oxidized during the fabrication process. It is clear that the intensity of copper oxide peaks decreases and disappears consequently after Si deposition and $H_2$ annealing. There are no obvious diffraction peaks associated with Si in the XRD patterns, suggesting the state of Si in the electrode is mainly amorphous. In an early report, Song *et al.* claimed the amorphous Si is more feasible to form crystallization alloy with Li ions [23]. The

existence of amorphous Si is in good accordance with TEM images (Fig. 4c-d). The EDS elemental mapping not only shows the Si deposited on the porous MWCNTs/Cu NWs-coated Cu foil, but also demonstrates the uniformly distribution of all the elements in the MCS5 composite electrode as seen in Fig. 6.

Fig. 7a-b show the charge and discharge capacities versus cycle numbers for PCS (pure Cu NWs/Si), PMS (pure MWCNTs/Si), and MCS composite electrodes including MCS1 (MWCNTs: Cu NWs = 1:1), MCS5 (MWCNTs: Cu NWs = 1:5), and MCS10 (MWCNTs: Cu NWs = 1:10) scanned at 1 A $g^{-1}$ and 3.5 A $g^{-1}$, respectively, as well as the correlative Coulombic efficiencies. The cycling performance in Fig. 7a was directly performed at 1 A $g^{-1}$ without pre-cycling. Therefore, the first three Coulombic efficiencies of all electrodes are commonly lower than following efficiencies, which is related to the unstable and inactivated electrochemical performance of the batteries. It is clear that the MCS10 electrode exhibits the highest reversible capacity of 1953 mAh $g^{-1}$ and remains the largest capacity retention of 93.4 % after 180 cycles. Compared with the MCS10 electrode, the PCS, PMS, MCS1, and MCS5 electrodes present slightly lower reversible capacities at fourth cycle (1380, 1499, 1575, and 1953 mAh $g^{-1}$) and the correlative capacity retentions of 98.9 %, 76.1 %, 98.7 %, and 80.8 % after 176 cycles. It is worth noting that PCS electrode shows a more stable cycling trend than that in Fig. 3c, because the dispersion agent of Cu NWs suspension was changed from DI water to IPA. Cu NWs disperse more evenly in IPA than DI water, resulting in a more uniform distribution of Cu NWs on Cu foils. In contrast with the PCS electrode, the PMS electrode has higher initial discharge and charge capacity, but suffers a quick capacity drop to 900 mAh $g^{-1}$ after 180 cycles. Although Cu NWs are inert for lithiation while MWCNTs are lithiation active materials with high capacitance, the MWCNTs coated on Cu foils contribute very little to the capacity due to the low weight (Fig. S3). In addition, the MWCNTs has larger resistivity than Cu NWs, which consequently reduces the electrical contact between the active material and current collector and retards the rapid electron transmission. Thus, the concentration of MWCNTs in the MWCNTs/Cu NWs/Si composite electrodes has a crucial effect on the electrochemical performance. For example, in the MCS1 electrode, the MWCNTs account for 50 % weight of the spin-coating layer, which greatly decreases the electrical contact between active materials and Cu foils than PCS electrodes. Besides, the excessive flexible MWCNTs

might fill up the pores creased by cross-linked Cu NWs, leading to lower porosity of current collector. Therefore, Si tends to deposit on the surface rather than form the core-shell structure with nanowires and nanotubes. In other words, there is less empty space available to accommodate the volume expansion of Si [30]. Therefore, among MWCNTs/Cu NWs/Si electrodes, MCS1 has the lowest capacity.

To understand the cycling performance of these electrodes at a higher rate, the MCS electrodes were tested at 3.5 A $g^{-1}$ shown in Fig. 7b. Initially, the curves suddenly decrease to 633, 651, 676, 841, and 803 mAh $g^{-1}$ in accordance with PCS, PMS, MCS1, MCS5, and MCS10 electrodes. The huge charge/discharge current density results in the low transport efficiency of Li ions, which finally leads to the small capacities of all electrodes at the beginning. After three or four cycles, the batteries tend to be stable and the specific capacity starts to increase gradually until achieving a full Li ions storage capacity [32]. The highest reversible capacities for each electrode (PCS, PMS, MCS1, MCS5, and MCS10) are 1523, 1128, 1521, 1719, and 1845 mAh $g^{-1}$ with corresponding capacity retentions of 93.9 %, 87.7 %, 96.3 %, 89.9 %, and 85.1 %, respectively. Likewise, the MCS10 electrode has the lowest capacity retention, and it possesses the highest charge and discharge capacity during 180 cycles.

To assess the rate capability of the MCS electrodes, the batteries were tested with increasing current densities by a step of 0.2, 0.5, 1, 1.5, 2, 2.5, to 3 A $g^{-1}$ and repeated steps, as illustrated in Fig. 7c. The composites (MCS1 and MCS5) show lower capacities than that of the PCS electrode. However, the MCS10 electrode still remains the highest reversible capacity due to the high concentration of conductive Cu NWs in the electrode. The little fluctuation observed during the first seven rates disappears in the next seven rates, which is ascribed to the instability and inactivation of the batteries at the beginning of the test. When the current density first returns to 0.2 A $g^{-1}$, the PCS, MCS1, MCS5, and MCS10 composite deliver capacities of 2289, 1841, 2031, and 2589 mAh $g^{-1}$ respectively that are very approaching the initial discharge capacity. Meanwhile, the capacity of MCS10 electrode even exceeds the initial value. Inspiringly, when the current density backs to 0.2 A $g^{-1}$ again, the discharge capacities achieve 2081, 1374, 1563, and 2251 mAh $g^{-1}$ for the PCS, MCS1, MCS5, and MCS10 composites with retentions of 90.9 %, 74.6 %, 77.0 %, and 86.9 %, respectively. The good capacity retentions indicate a good stability of the electrode after high-rate

discharge-charge cycles, which can highlight the excellent Li-ion storage reversibility. Further experiments were conducted to compare the rate performance of MCS10, MCS15, and MCS50 as shown in Fig. S4, in which the electrochemical performance decreases when the weight ratio of MWCNTs and Cu NWs decreases from 1:10 to 1:50. Therefore, among the MWCNTs/Cu NWs/Si composite electrodes, the optimal ratio of MWCNTs and Cu NWs is found to be 1:10.

To further investigate the stable cycling performance of 3D composite electrodes, the PCS, PMS, and MCS10 anodes after 100 charge/discharge cycles were characterized by SEM in Fig. 8 (the corresponding SEM images before cycling are shown in Fig. S5). As presented in Fig. 8a, the PCS composite generates huge cracks, of which the width is approximately several micrometers. The exfoliation of active materials from current collector indicates the electrical contact loss, which explains the rapid attenuation in capacity of anodes after 100 cycles. By comparison, there are similar cracks on the PMS electrodes, but no obvious exfoliation is discovered in Fig. 8b, which is attributed to the robust MWCNTs stabilizing the 3D structure of the electrode. Among these three 3D-structure electrodes, MCS10 maintains the original integrity and stability without significant deformation or breakages (Fig. 8c). The partial enlarge view in Fig. 8d demonstrates the stability of MWCNTs/Cu NWs/Si structure, indicating its efficiency to buffer the volume expansion of silicon.

In general, the robust MWCNTs could strengthen the stability of the composite electrode, on the other hand, the superior conductivity of Cu NWs increases the specific capacity to a large extent. In addition, the concentration of MWCNTs is associated with the porosity factor of current collector for Si deposition, which is critical for the cyclic stability performance of the electrode. Among all electrodes with different weight ratios, the MCS10 electrode shows the best electrochemical performance, implying that the ratio of MWCNTs and Cu NWs achieves the optimized balance.

## 4. Conclusions

In conclusion, MWCNTs/Cu NWs/Si composites have been successfully fabricated by spin-coating and PECVD. The 3D MWCNTs/Cu NWs coated on current collector serves as a matrix for Si deposition accommodating the volume change of Si during

charge/discharge cycles and accelerating the transmission of Li ions between electrodes. The MWCNTs/Si and Cu/Si core-shell presents remarkable structural features with enhanced conductivity, shortened the Li ions diffusion distance, and more active area for electrochemical reactions. As a consequence, MWCNTs/Cu NWs/Si composite electrode exhibits improved lithium storage properties in terms of high capacity, long cycle life, and good rate performance. All these results highlight that the rational selection and design of the MWCNTs/Cu NWs/Si composite electrode might allow it to be developed as an advanced anode materials LIBs.

## Acknowledgments

This work was supported by the National Natural Science Foundation of China (NSFC Grants 21750110441), Suzhou Industrial Park Initiative Platform Development for Suzhou Municipal Key Lab for New Energy Technology (RR0140), and Key Program Special Fund in XJTLU (KSF-A-04).

# References

[1] W.J. Zhang, A review of the electrochemical performance of alloy anodes for lithium-ion batteries, Journal of Power Sources, 196 (2011) 13-24.

[2] A.L. Michan, G. Divitini, A.J. Pell, M. Leskes, C. Ducati, C.P. Grey, Solid electrolyte interphase growth and capacity loss in silicon electrodes, Journal of the American Chemical Society, 138 (2016) 7918-7931.

[3] H. Wu, Y. Cui, Designing nanostructured Si anodes for high energy lithium ion batteries, Nano Today, 7 (2012) 414-429.

[4] T. Mu, P. Zuo, S. Lou, Q. Pan, H. Zhang, C. Du, Y. Gao, X. Cheng, Y. Ma, H. Huo, G. Yin, A three-dimensional silicon/nitrogen-doped graphitized carbon composite as high-performance anode material for lithium ion batteries, Journal of Alloys and Compounds, 777 (2019) 190-197.

[5] H. Wu, G. Chan, J.W. Choi, I. Ryu, Y. Yao, M.T. McDowell, S.W. Lee, A. Jackson, Y. Yang, L. Hu, Y. Cui, Stable cycling of double-walled silicon nanotube battery anodes through solid-electrolyte interphase control, Nature Nanotechnology, 7 (2012) 309-314.

[6] X. Su, Q. Wu, J. Li, X. Xiao, A. Lott, W. Lu, B.W. Sheldon, J. Wu, Silicon-based nanomaterials for lithium-ion batteries: a review, Advanced Energy Materials, 4 (2014).

[7] M.V. Shelke, H. Gullapalli, K. Kalaga, M.-T.F. Rodrigues, R.R. Devarapalli, R. Vajtai, P.M. Ajayan, Facile synthesis of 3D anode assembly with Si nanoparticles sealed in highly pure few layer graphene deposited on porous current collector for long life Li-ion battery, Advanced Materials Interfaces, 4 (2017) 1601043.

[8] H.T. Nguyen, F. Yao, M.R. Zamfir, C. Biswas, K.P. So, Y.H. Lee, S.M. Kim, S.N. Cha, J.M. Kim, D. Pribat, Highly interconnected Si nanowires for improved stability Li-ion battery anodes, Advanced Energy Materials, 1 (2011) 1154-1161.

[9] C.K. Chan, H. Peng, G. Liu, K. McIlwrath, X.F. Zhang, R.A. Huggins, Y. Cui, High-performance lithium battery anodes using silicon nanowires, Nature Nanotechnology, 3 (2007) 31.

[10] Z. Zhou, P. Dong, D. Wang, M. Liu, J. Duan, G.P. Nayaka, D. Wang, C. Xu, Y. Hua, Y. Zhang, Silicon-titanium nanocomposite synthesized via the direct electrolysis of $SiO_2/TiO_2$ precursor in molten salt and their performance as the anode material for lithium ion batteries, Journal of Alloys and Compounds, 781 (2019) 362-370.

[11] H. Wu, G. Zheng, N. Liu, T.J. Carney, Y. Yang, Y. Cui, Engineering empty space between Si nanoparticles for lithium-ion battery anodes, Nano Letters, 12 (2012)

904-909.

[12] L. Sun, F. Wang, T. Su, H.B. Du, Step-by-step assembly preparation of core-shell Si-mesoporous $TiO_2$ composite nanospheres with enhanced lithium-storage properties, Dalton Trans, 46 (2017) 11542-11546.

[13] Y. Yao, Y. Zhu, S. Zhao, J. Shen, X. Yang, C. Li, Halide ion intercalated electrodeposition synthesis of $Co_3O_4$ nanosheets with tunable pores on graphene foams as free-standing and flexible Li-ion battery anodes, ACS Applied Energy Materials, 1 (2018) 1239-1251.

[14] C. Shen, X. Fang, M. Ge, A. Zhang, Y. Liu, Y. Ma, M. Mecklenburg, X. Nie, C. Zhou, Hierarchical carbon-coated ball-milled silicon: synthesis and applications in free-standing electrodes and high-voltage full lithium-ion batteries, ACS Nano, (2018).

[15] N. Wang, T. Hang, H. Ling, A. Hu, M. Li, High-performance Si-based 3D Cu nanostructured electrode assembly for rechargeable lithium batteries, Journal of Materials Chemistry A, 3 (2015) 11912-11919.

[16] Z. Zhang, Z.L. Wang, X. Lu, Multishelled Si@Cu microparticles supported on 3D Cu current collectors for stable and binder-free anodes of lithium-ion batteries, ACS Nano, 12 (2018) 3587-3599.

[17] S. Li, W. Xie, L. Gu, Z. Liu, X. Hou, B. Liu, Q. Wang, D. He, Facilely scraping Si nanoparticles@reduced graphene oxide sheets onto nickel foam as binder-free electrodes for lithium ion batteries, Electrochimica Acta, 193 (2016) 246-252.

[18] Y. Liu, K. Huang, Y. Fan, Q. Zhang, F. Sun, T. Gao, Z. Wang, J. Zhong, Binder-free Si nanoparticles@carbon nanofiber fabric as energy storage material, Electrochimica Acta, 102 (2013) 246-251.

[19] B. Liu, X. Wang, H. Chen, Z. Wang, D. Chen, Y.-B. Cheng, C. Zhou, G. Shen, Hierarchical silicon nanowires-carbon textiles matrix as a binder-free anode for high-performance advanced lithium-ion batteries, Scientific Reports, 3 (2013) 1622.

[20] X. Ma, L. Chen, X. Ren, G. Hou, L. Chen, L. Zhang, B. Liu, Q. Ai, L. Zhang, P. Si, J. Lou, J. Feng, L. Ci, High-performance red phosphorus/carbon nanofibers/graphene free-standing paper anode for sodium ion batteries, Journal of Materials Chemistry A, 6 (2018) 1574-1581.

[21] H. Wang, H. Song, Z. Lin, X. Jiang, X. Zhang, L. Yu, J. Xu, L. Pan, J. Wang, M. Zheng, Y. Shi, K. Chen, Highly cross-linked Cu/a-Si core-shell nanowires for ultra-long cycle life and high rate lithium batteries, Nanoscale, 8 (2016) 2613-2619.

[22] H. Guan, X. Wang, S. Chen, Y. Bando, D. Golberg, Coaxial Cu-Si@C array

electrodes for high-performance lithium-ion batteries, Chemical Communications, 47 (2011) 12098-12100.

[23] H. Song, H.X. Wang, Z. Lin, X. Jiang, L. Yu, J. Xu, Z. Yu, X. Zhang, Y. Liu, P. He, L. Pan, Y. Shi, H. Zhou, K. Chen, Highly connected silicon–copper alloy mixture nanotubes as high-rate and durable anode materials for lithium-ion batteries, Advanced Functional Materials, 26 (2016) 524-531.

[24] H. Song, H.X. Wang, Z. Lin, L. Yu, X. Jiang, Z. Yu, J. Xu, L. Pan, M. Zheng, Y. Shi, K. Chen, Hierarchical nano-branched c-Si/$SnO_2$ nanowires for high areal capacity and stable lithium-ion battery, Nano Energy, 19 (2016) 511-521.

[25] Q. Zhang, H. Chen, L. Luo, B. Zhao, H. Luo, X. Han, J. Wang, C. Wang, Y. Yang, T. Zhu, M. Liu, Harnessing the concurrent reaction dynamics in active Si and Ge to achieve high performance lithium-ion batteries, Energy & Environmental Science, 11 (2018) 669-681.

[26] Y. Chang, M.L. Lye, H.C. Zeng, Large-scale synthesis of high-quality ultralong copper nanowires, Langmuir, 21 (2005) 3746-3748.

[27] L. Lin, Y. Ma, Q. Xie, L. Wang, Q. Zhang, D. Peng, Copper-nanoparticle-induced porous Si/Cu composite films as an anode for lithium ion batteries, ACS Nano, 11 (2017) 6893-6903.

[28] D.B. Polat, O. Keles, K. Amine, Well-aligned, ordered, nanocolumnar, Cu–Si thin film as anode material for lithium-ion batteries, Journal of Power Sources, 270 (2014) 238-247.

[29] H. Zhang, S. Jing, Y. Hu, H. Jiang, C. Li, A flexible freestanding Si/rGO hybrid film anode for stable Li-ion batteries, Journal of Power Sources, 307 (2016) 214-219.

[30] Z. Yin, S. Cho, D.-J. You, Y.-k. Ahn, J. Yoo, Y.S. Kim, Copper nanowire/multi-walled carbon nanotube composites as all-nanowire flexible electrode for fast-charging/discharging lithium-ion battery, Nano Research, 11 (2017) 769-779.

[31] H. Wu, N. Du, H. Zhang, D. Yang, Voltage-controlled synthesis of Cu-$Li_2O$@Si core-shell nanorod arrays as high-performance anodes for lithium-ion batteries, Journal of Materials Chemistry A, 2 (2014) 20510-20514.

[32] M. Liu, X. Deng, Y. Ma, W. Xie, X. Hou, Y. Fu, D. He, Well-designed hierarchical $Co_3O_4$ architecture as a long-life and ultrahigh rate capacity anode for advanced lithium-ion batteries, Advanced Materials Interfaces, 4 (2017) 1700553.

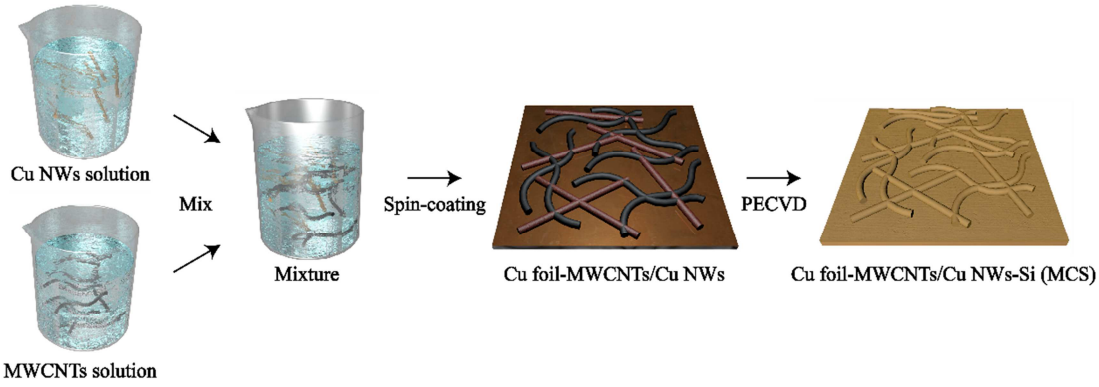


**Fig. 1.** Schematic illustration showing the preparation procedure of the MWCNTs/Cu NWs/Si (MCS) composite electrode.

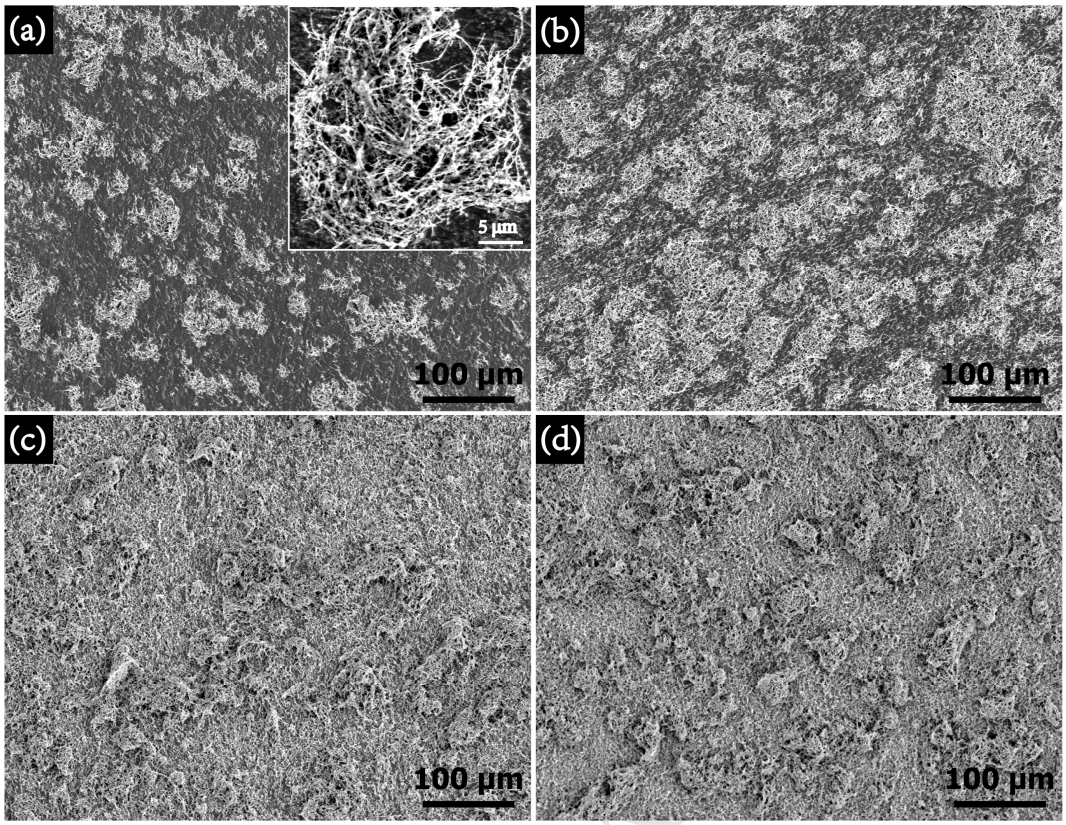


**Fig. 2.** SEM images of pure Cu NWs-coated Cu foils as porous current collectors with 2 (a), 5 (b), 8 (c), and 12 (d) layers of Cu NWs by spin-coating.

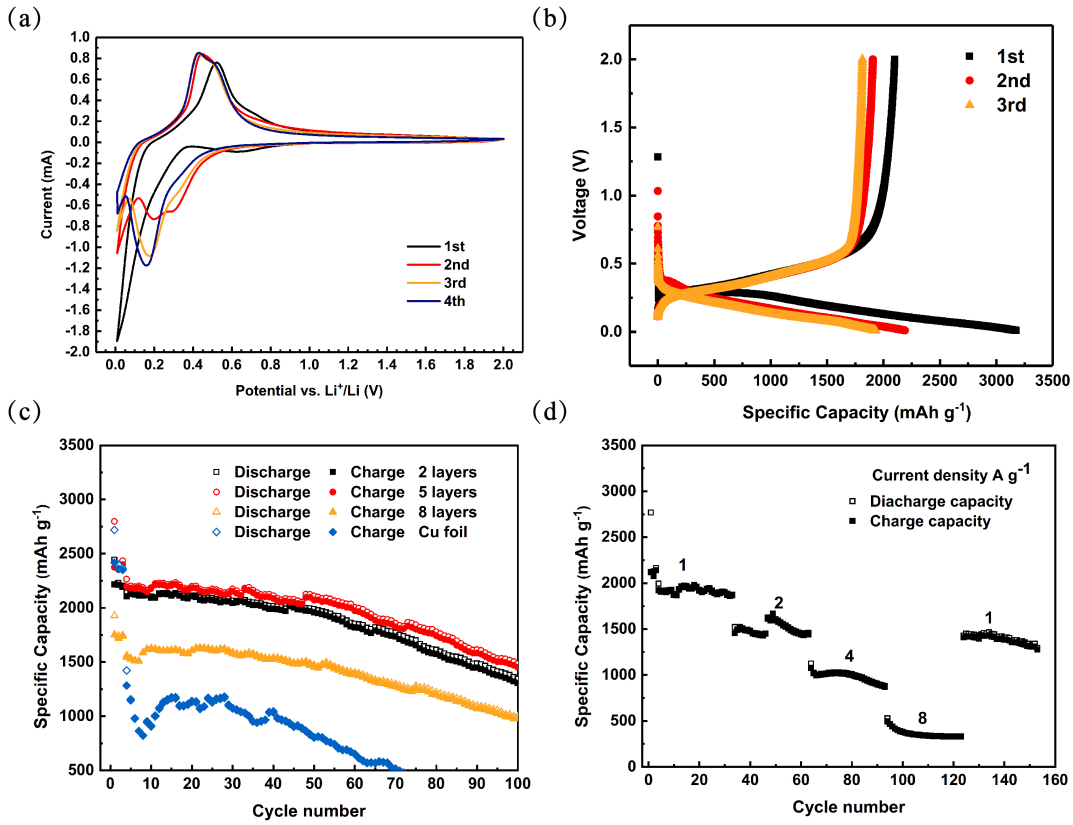


**Fig. 3.** (a) Cyclic voltammetry curves for the first four cycles of PCS composite electrode with 5 spin-coated layers of Cu NWs at a scan rate of 0.1 mV $s^{-1}$ with the voltage range of 0.01-2.0 V; (b) voltage profiles with first three cycles of PCS composite electrode with 5 coating layers at a current density of 0.42 A $g^{-1}$; (c) cycling performance of PCS composite electrodes with different spin-coated layers at 1 A $g^{-1}$; (d) rate performance of the PCS composite electrode with 5 coating layers.

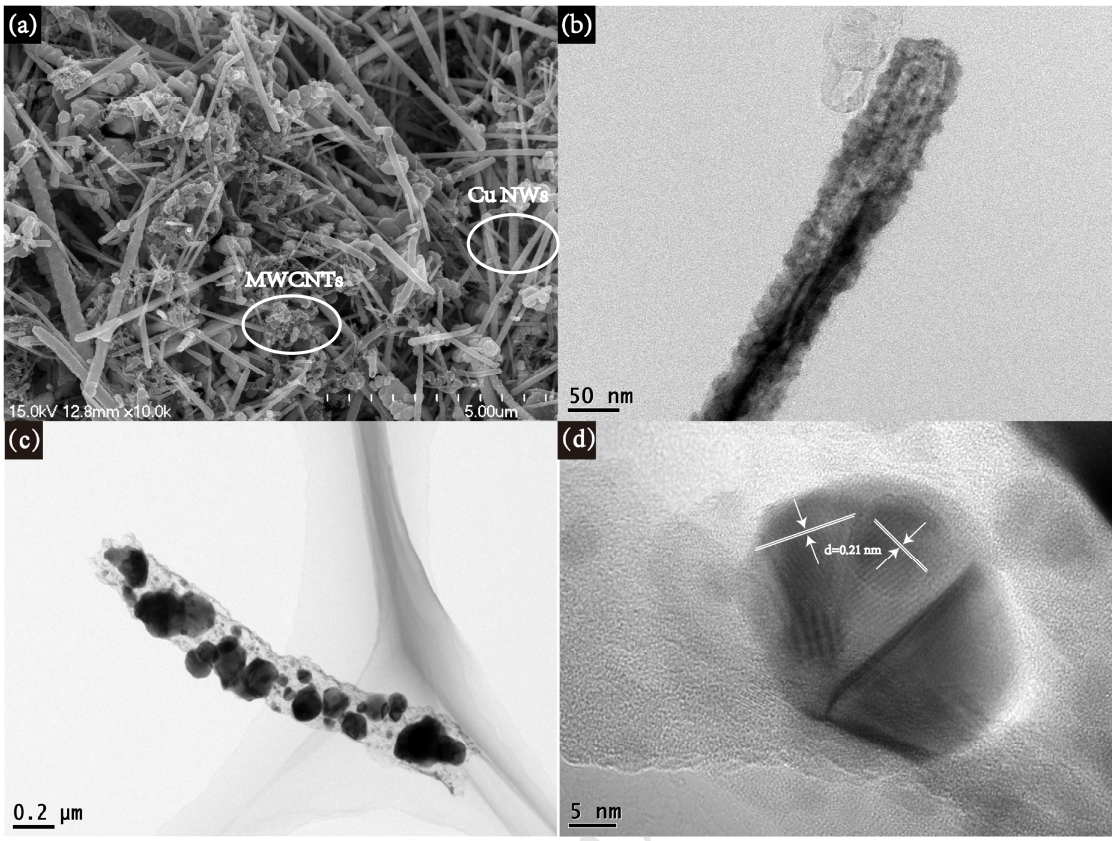


**Fig. 4.** (a) SEM image of MCS1 composite electrode with 5 layers of MWCNTs/Cu NWs; (b) TEM image of Cu NWs@Si core-shell structure before annealing; TEM images of Cu NWs@Si after annealing (c) with the partial enlarged HRTEM views (d).

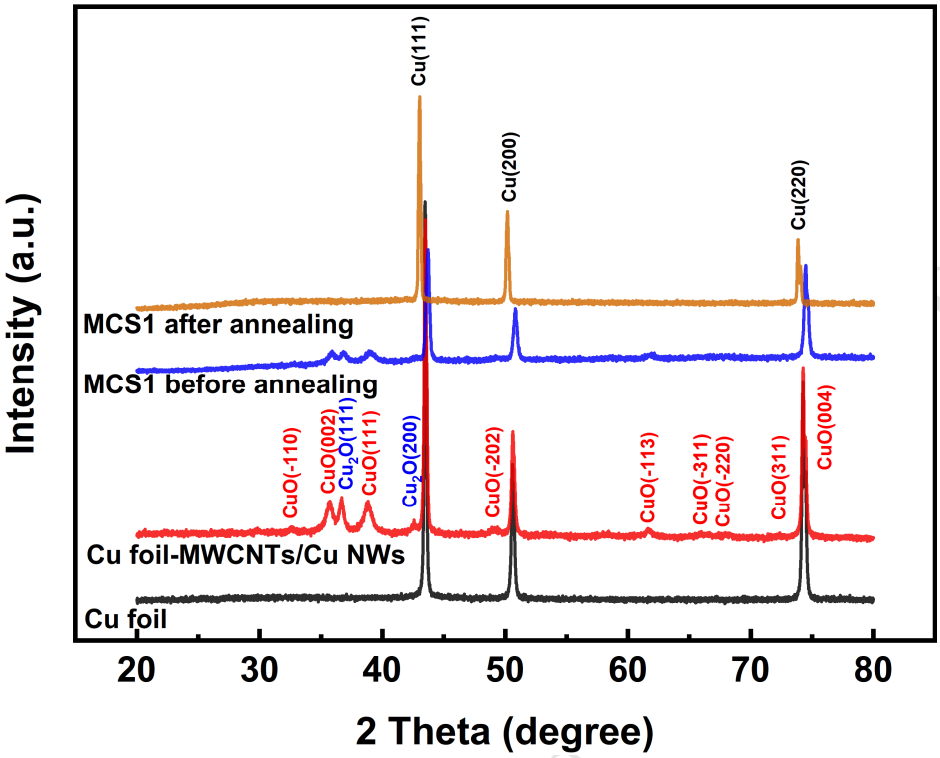


**Fig. 5.** XRD patterns of the Cu foil (black), Cu foil coated by 5 layers of MWCNTs/Cu NWs (MWCNTs:Cu NWs=1:1) (red), MCS1 composite electrode before (blue) and after (brown) annealing.

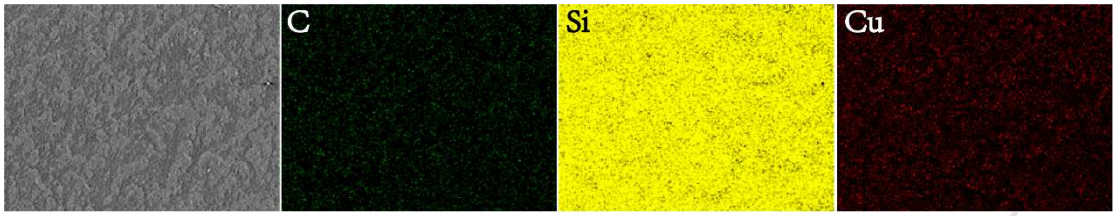


**Fig. 6.** EDS elemental mappings of MCS5 composite electrode with 5 layers of MWCNTs/Cu NWs on Cu foils.

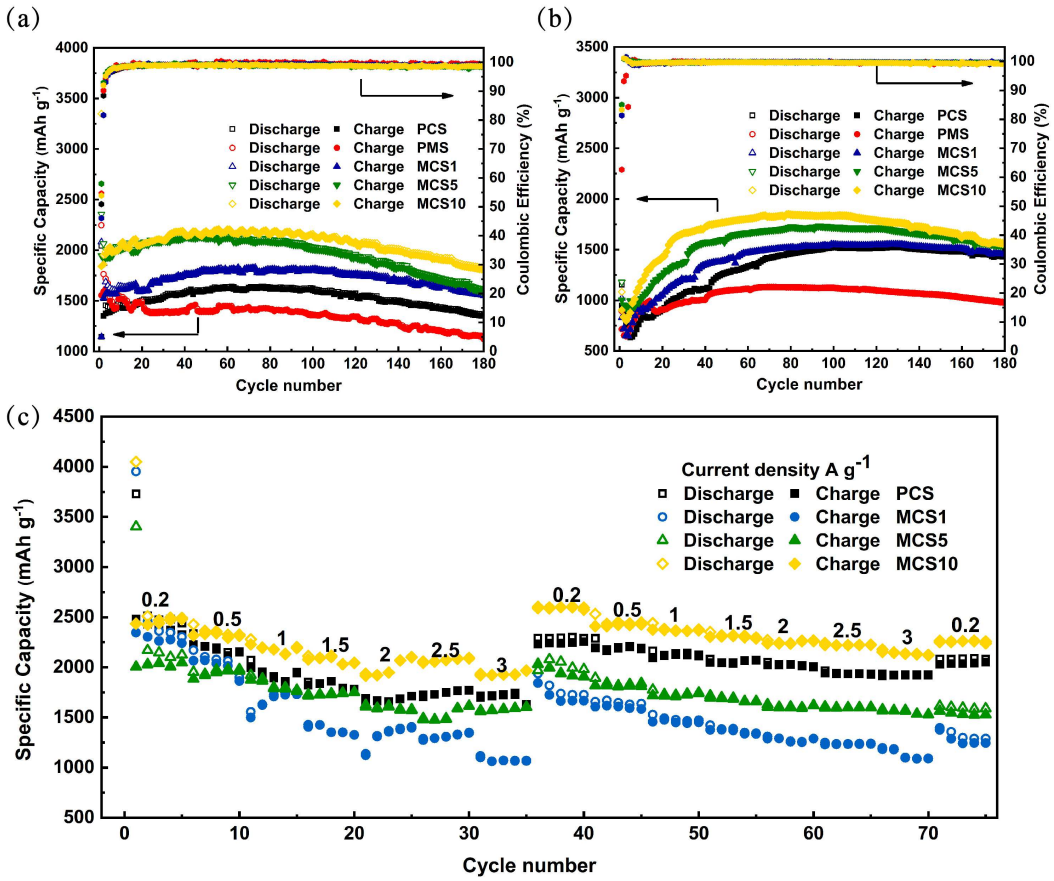


**Fig. 7.** Cycling performance of PCS, PMS, and MCS composite electrodes with different weight ratios of MWCNTs and Cu NWs (with 5 layers of MWCNTs/Cu NWs) at 1 A $g^{-1}$ (a) and 3.5 A $g^{-1}$ (b); (c) rate performance of the MCS composite electrodes.

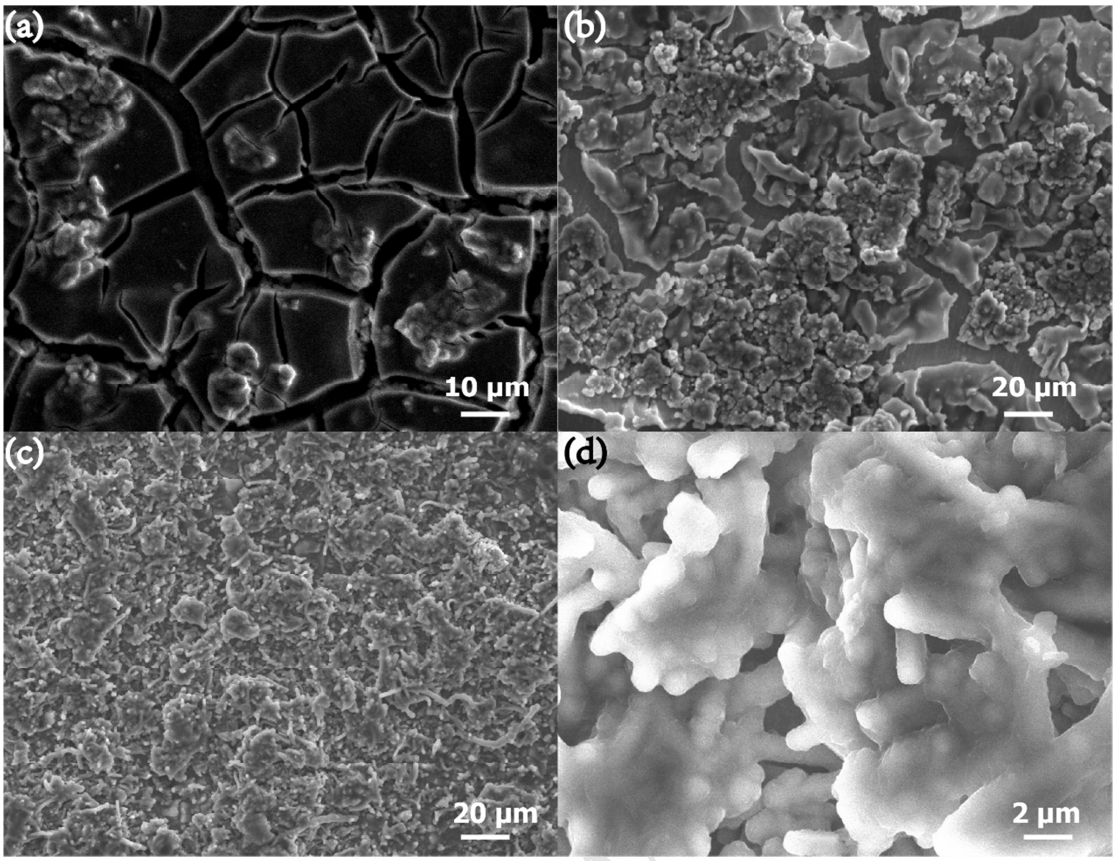


**Fig. 8.** SEM images of 3D-structured PCS (a), PMS (b), and MCS10 (c-d) composite electrodes with 5 spin-coated layers after 100 cycles.

1. Three-dimensional multi-walled carbon nanotubes/copper nanowires composite-coated current collector was prepared by spin-coating.
2. Amorphous Si film was deposited by a plasma-enhanced chemical vapor deposition on the three-dimensional porous current collector.
3. The highly conductive copper nanowires cooperate with robust multi-walled carbon nanotubes to create numerous voids on the surface of copper foils to improve the cycling performance of the batteries.